IEEE Access
Multidisciplinary | Rapid Review | Open Access Journal

Received 12 January 2024, accepted 23 January 2024, date of publication 30 January 2024, date of current version 14 February 2024.

Digital Object Identifier 10.1109/ACCESS.2024.3360038

RESEARCH ARTICLE

State Machine-Based Waveforms for Channels With 1-bit Quantization and Oversampling With Time-Instance Zero-Crossing Modulation

DIANA MARCELA V. MELO, (Member, IEEE), LUKAS T. N. LANDAU, (Senior Member, IEEE), AND RODRIGO C. DE LAMARE, (Senior Member, IEEE)

Departamento de Engenharia Elétrica (DEE), Pontifícia Universidade Católica do Rio de Janeiro (PUC-Rio), Rio de Janeiro 22451-900, Brazil

Corresponding author: Diana Marcela V. Melo (diana@aluno.puc-rio.br)

ABSTRACT Systems with 1-bit quantization and oversampling are promising for the Internet of Things (IoT) networks because they can reduce the power consumption of the analog-to-digital-converters in the devices. The novel time-instance zero-crossing (TI ZX) modulation is a promising approach for IoT networks and devices but existing studies rely on optimization problems with high computational complexity and delay. In this work, we propose a practical waveform design based on the established TI ZX modulation for a multiuser multi-input multi-output (MIMO) systems in the downlink scenario with 1-bit quantization and temporal oversampling at the receivers. In this sense, the proposed temporal transmit signals are constructed by concatenating segments of coefficients which convey the information into the time-instances of zero-crossings according to the TI ZX mapping rules. The proposed waveform design is compared with other methods from the literature in terms of bit error rate and normalized power spectral density. Numerical results show that the proposed technique is suitable for multiuser MIMO systems with 1-bit quantization while tolerating some small amount of out-of-band radiation.

INDEX TERMS Zero-crossing precoding, oversampling, Moore machine, 1-bit quantization.

I. INTRODUCTION

Future wireless communication technologies are envisioned to support a large number of the Internet of Things (IoT) devices which require to have low power consumption and low complexity. Low resolution analog-to-digital converters (ADCs) that equip IoT devices are suitable to meet the requirements since the power consumption in the ADCs increases exponentially with its amplitude resolution [1]. Moreover, the loss of information caused by the coarse quantization can be partially compensated by increasing the sampling rate. In particular, by employing temporal M_{Rx}-fold oversampling, rates of $\log_2(M_{\mathrm{Rx}}+1)$ bits per Nyquist interval are achievable in a noise free environment [2]. The authors in [3] studied the maximization of the achievable rate for systems with 1-bit quantization and oversampling in the presence of noise. Other studies that considered systems with 1-bit quantization and oversampling employ ASK transmit sequences [4], [5], [6] and 16 QAM modulation [7]. Other practical methods are based on the idea presented in [2], where the information is conveyed into the zero-crossings. An example is the study presented in [8], where the waveform is constructed by concatenating sequences which convey the information into the zero-crossings. This study shows that similar data rates to the one presented in [2] can be achieved over noisy channels with relatively low out-of-band radiation. Some other practical methods which convey the information into the zero-crossings include runlength-limited (RLL) sequences [9], [10]. Other modern methods that consider the reduction of energy consumption in the

The associate editor coordinating the review of this manuscript and approving it for publication was Poki Chen.

ADCs are based on sub-Nyquist sampling methods such as the one presented in [11].

The benefits of 1-bit quantization and oversampling have been studied in [12] and [13] for multiuser multiple-input multiple-output (MIMO) systems in uplink scenarios. Moreover, the studies in [14] and [15] have investigated sequences for downlink MIMO systems with 1-bit quantization and oversampling. In this regard, in [14] it is presented a quantized precoding method which considers as optimization criterion the maximization of the minimum distance to the decision threshold (MMDDT) which is a well-established design criterion in literature [7], [16], [17], [18], and [19], that is mathematically tractable and suitable for low-resolution techniques. In [17] this design criterion is known as a safety margin to the decision thresholds and in [19] the minimum distance is considered as a quality-of-service (QoS) design criterion. The quantized precoding technique of [14] relies on an exhaustive codebook search which allows simple Hamming distance detection. Superior precoding schemes to those of [14] for MIMO downlink scenarios have been investigated in [20], where a novel time-instance zero-crossing (TI ZX) modulation was introduced. This novel modulation follows the idea of [2] by allocating the information into the time-instance of zero-crossings in order to reduce the number of zero-crossings of the signal. In this sense, the proposed TI ZX waveform is tailored for systems with 1-bit quantization and oversampling.

The study in [20] relied on a precoding technique based on the MMDDT criterion with spatial zero-forcing (ZF) precoding and TI ZX modulation. Moreover, [20] proposed an optimal temporal-spatial precoding technique with TI ZX modulation along with a minimum mean square error (MMSE) solution. Other studies that consider novel TI ZX modulation schemes have been presented in [15], [21], and [22] where the computational complexity is reduced [21]. In [22] the minimization of the transmit power under a quality of service constraint was considered as an objective. The study in [15] investigated the spectral efficiency of MIMO systems with sequences constructed with the TI ZX modulation and RLL sequences.

In general, the TI ZX modulation allows a lower number of zero crossings in comparison with other methods from the literature such as the QP method [14] and the transceiver design from [8]. A lower number of zero-crossings allows for relaxation in the waveform design. Moreover, in comparison with other methods such as RLL sequences, the TI ZX modulation yields a lower detection complexity since a Viterbi decoder is not required while having a comparable spectral efficiency. Note that, the TI ZX modulation achieves a higher data rate in comparison with conventional modulation schemes such as QPSK, where a maximum rate of 2 bits per Nyquist interval can be achieved, while For TI ZX modulation with $M_{\mathrm{Rx}} = 2$, approximately 3 bits per Nyquist interval are achieved and for $M_{\mathrm{Rx}} = 3$, approximately 4 bits per Nyquist interval are achieved. Due to the simple architecture and low power consumption, it is promising for battery driven IoT receivers. In this context, the main idea of the proposed scheme is to shift the complexity from the IoT devices to the base station.

In this work, we propose a TI ZX waveform design for multiuser MIMO systems in downlink scenarios with 1-bit quantization and oversampling where a predefined level of out-of-band radiation is tolerated. The proposed waveform design considers the novel TI ZX modulation from [20] and follows a similar idea as presented in [8]. The proposed method conveys the information into the time-instances of zero-crossings but instead of considering sequences of samples, input bits are mapped into waveform segments according to the TI ZX mapping rules [20]. The temporal precoding vector is then used in conjunction with a simple pulse shaping filter. The optimal set of coefficients is computed with an optimization problem which is formulated to maximize the minimum distance to the decision threshold, constrained with some tolerated out-of-band radiation. Finally, the numerical results are evaluated considering the bit error rate (BER) and the power spectral density (PSD). The proposed waveform design is compared with the transceiver waveform design from [8] and the TI ZX MMDDT precoding [20]. The transceiver waveform design [8] was adapted for MIMO channels. The simulation results show that the proposed waveform design is comparable in terms of BER performance to the one presented for TI ZX MMDDT precoding while having a lower computational complexity since the waveform optimization is done once and is suitable for any input sequence of bits.

The rest of the paper is organized as follows: The system model is introduced in Section II. Then, Section III describes the novel TI ZX modulation. Section IV explains the proposed waveform design optimization including the autocorrelation function for TI ZX modulated sequences. Section V presents a practical waveform design optimization strategy. The simulation results are provided in Section VI and finally, the conclusions are given in Section VII.

Notation: In the paper all scalar values, vectors and matrices are represented by: a, $\boldsymbol{x}$ and $\boldsymbol{X}$, respectively.

II. SYSTEM MODEL

In this study, a multiuser MIMO downlink scenario with N_{u} single antenna users and N_{t} transmit antennas at the base station (BS), is considered as shown in Fig. 1. The input sequence of bits $\boldsymbol{x}_{b_k}$ for user k is mapped into the sequences of symbols $\boldsymbol{x}_k$, such that transmission blocks of N symbols (N Nyquist intervals) are considered. The input sequence for user k is mapped using the TI ZX mapping and the set of coefficients $\mathcal{G}$ which yields the temporal precoding vector $\boldsymbol{s}_{g_k} \in \mathbb{C}^{N_{\mathrm{tot}}}$, where $N_{\mathrm{tot}} = M_{\mathrm{Rx}}N$ and M_{Rx}/T denotes the sampling rate and T refers to the symbol duration. Moreover, the transmit filter $g_{\mathrm{Tx}}(t)$ and receive filter $g_{\mathrm{Rx}}(t)$ are presented, where the combined waveform is given by $v(t) = (g_{\mathrm{Tx}} * g_{\mathrm{Rx}})(t)$. Furthermore 1-bit quantization is applied at the receivers. The channel matrix $\boldsymbol{H} \in \mathbb{C}^{N_{\mathrm{u}} \times N_{\mathrm{t}}}$

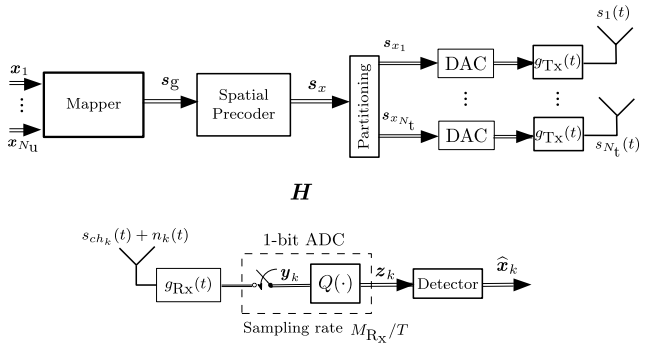

FIGURE 1. Considered multi-user MIMO downlink system model.

is known at the base station and is considered to be frequency-flat fading as typically assumed for narrowband IoT systems [14]. Then, stacking the temporal precoding vector of all the N_{u} users, the temporal precoding vector $\boldsymbol{s}_g$ is otained such that $\boldsymbol{s}_g = \left[\boldsymbol{s}_{g_1}^T, \boldsymbol{s}_{g_2}^T, \cdots, \boldsymbol{s}_{gk}^T, \cdots, \boldsymbol{s}_{gN_{\mathrm{u}}}^T\right]^T$. The process to obtain the temporal precoding vector $\boldsymbol{s}_{gk}$ is explained in Section IV.

The received signal $\boldsymbol{z} \in \mathbb{C}^{N_{\mathrm{tot}}N_{\mathrm{u}}}$ can be expressed by stacking the received samples of the N_{u} users as follows:

$$\begin{aligned}\boldsymbol{z} &= Q_1\left(\left(\boldsymbol{H}\boldsymbol{P}_{\mathrm{sp}} \otimes \boldsymbol{I}_{N_{\mathrm{tot}}}\right)\left(\boldsymbol{I}_{N_{\mathrm{u}}} \otimes \boldsymbol{V}\right)\boldsymbol{s}_{\mathrm{g}} + \left(\boldsymbol{I}_{N_{\mathrm{u}}} \otimes \boldsymbol{G}_{\mathrm{Rx}}\right)\boldsymbol{n}\right) \\ &= Q_1\left(\left(\boldsymbol{H}\boldsymbol{P}_{\mathrm{sp}} \otimes \boldsymbol{V}\right)\boldsymbol{s}_{\mathrm{g}} + \left(\boldsymbol{I}_{N_{\mathrm{u}}} \otimes \boldsymbol{G}_{\mathrm{Rx}}\right)\boldsymbol{n}\right) \\ &= Q_1\left(\boldsymbol{H}_{\mathrm{eff}}\boldsymbol{s}_{\mathrm{g}} + \boldsymbol{G}_{\mathrm{Rx,eff}}\boldsymbol{n}\right), \end{aligned} \tag{1}$$

where $Q_1(\cdot)$ corresponds the 1-bit quantization operator, $\boldsymbol{n} \in \mathbb{C}^{3N_{\mathrm{tot}}N_{\mathrm{u}}}$ denotes a vector with zero-mean complex Gaussian noise samples with variance σ_n^2. The waveform matrix $\boldsymbol{V}$ with size $N_{\mathrm{tot}} \times N_{\mathrm{tot}}$ is given by

$$\boldsymbol{V} = \begin{bmatrix} v(0) & v\left(\frac{T}{M_{\mathrm{Rx}}}\right) & \cdots & v(TN) \\ v\left(-\frac{T}{M_{\mathrm{Rx}}}\right) & v(0) & \cdots & v\left(T\left(N-\frac{1}{M_{\mathrm{Rx}}}\right)\right) \\ \vdots & \vdots & \ddots & \vdots \\ v(-TN) & v\left(T\left(-N+\frac{1}{M_{\mathrm{Rx}}}\right)\right) & \cdots & v(0) \end{bmatrix}. \tag{2}$$

The receive filter g_{Rx} is represented in discrete time by the matrix $\boldsymbol{G}_{\mathrm{Rx}}$ with size $N_{\mathrm{tot}} \times 3N_{\mathrm{tot}}$ and is denoted as

$$\boldsymbol{G}_{\mathrm{Rx}} = a_{\mathrm{Rx}} \begin{bmatrix} \left[\boldsymbol{g}_{\mathrm{Rx}}^T\right] & 0 \cdots & 0 \\ 0 & \left[\boldsymbol{g}_{\mathrm{Rx}}^T\right] & 0 \cdots 0 \\ & \ddots\ddots\ddots & \\ 0 \cdots & 0 & \left[\boldsymbol{g}_{\mathrm{Rx}}^T\right] \end{bmatrix}, \tag{3}$$

with $\boldsymbol{g}_{\mathrm{Rx}} = [g_{\mathrm{Rx}}(-T(N+\frac{1}{M_{\mathrm{Rx}}})), g_{\mathrm{Rx}}(-T(N+\frac{1}{M_{\mathrm{Rx}}})+\frac{T}{M_{\mathrm{Rx}}}), \ldots, g_{\mathrm{Rx}}(T(N+\frac{1}{M_{\mathrm{Rx}}}))]^T$ and $a_{\mathrm{Rx}} = (T/M_{\mathrm{Rx}})^{1/2}$. The matrix $\boldsymbol{P}_{\mathrm{sp}} = c_{\mathrm{zf}}\boldsymbol{H}^{\mathrm{H}}\left(\boldsymbol{H}\boldsymbol{H}^{\mathrm{H}}\right)^{-1}$ denotes the spatial zero-forcing precoder. The matrix $\boldsymbol{P}_{\mathrm{sp}}$ is normalized such that the spatial precoder does not change the signal power. As in [20] the normalization factor c_{zf} is given by

$$c_{\mathrm{zf}} = \left(N_{\mathrm{u}}/\mathrm{trace}\left(\left(\boldsymbol{H}\boldsymbol{H}^{\mathrm{H}}\right)^{-1}\right)\right)^{\frac{1}{2}}. \tag{4}$$

TABLE 1. Zero-crossing assignment c_{map}.

c_{map}	
symbol	Zero-crossing assignment
b_1	No zero-crossing
b_2	Zero-crossing in the M_{Rx} interval
b_3	Zero-crossing in the $M_{\mathrm{Rx}}-1$ interval
$\vdots$	$\vdots$
$b_{R_{\mathrm{in}}-1}$	Zero-crossing in the second interval
$b_{R_{\mathrm{in}}}$	Zero-crossing in the first interval

III. TIME-INSTANCE ZERO-CROSSING MAPPING

The TI ZX modulation was proposed in [20] for systems with 1-bit quantization and oversampling. The TI ZX modulation conveys the information into the time instances of zero-crossings and also considers the absence of zero-crossing during a symbol interval as a valid symbol, different from [2] and [8]. The latter implies a lower average number of zero-crossings per Nyquist interval which results in a relaxation of the waveform design of systems with bandlimitation.

To build the mapped sequence, each input symbol x_i drawn from the set $\mathcal{X}_{\mathrm{in}} := \{b_1, b_2, \cdots, b_{R_{\mathrm{in}}}\}$ with $R_{\mathrm{in}} = M_{\mathrm{Rx}} + 1$, is mapped into a binary codeword $\boldsymbol{c}_{\mathrm{s}_i} \in \{-1, 1\}$ with M_{Rx} samples. The codeword $\boldsymbol{c}_{\mathrm{s}_i}$ determines the time instant within the symbol interval, in which the zero-crossing occurs or not. Once the codewords of all the transmit symbols have been generated, they are concatenated in one single vector, to generate the desired output pattern $\boldsymbol{c}_{\mathrm{out}}$. The construction of $\boldsymbol{c}_{\mathrm{out}}$ is done in the same way and separately for all the users, and the in-phase and quadrature components of the symbols. In the concatenation process, the last sample of the previous Nyquist interval, termed $\rho \in \{1, -1\}$, must be considered to map the next symbol into the corresponding binary codeword.

Due to ρ, each symbol b_j from the input alphabet is assigned to two different codewords which convey the same zero-crossing information. The mapping assignment $\boldsymbol{c}_{\mathrm{map}}$, shown in Table 1, relates each symbol b_j to its respective time instance zero-crossing where the information is conveyed.

Then, for coding and decoding of the first transmit symbol, a pilot sample $\rho_{\mathrm{b}} \in \{1, -1\}$ is required.

A. GRAY CODING FOR TIZX MODULATION

The Gray coding for TI ZX modulation established in [20] is considered such that symbols with consecutive or near zero-crossings differ only in one bit. For $M_{\mathrm{Rx}} = 3$, a binary tuple is mapped on one symbol. Sequences of symbols are considered for $M_{\mathrm{Rx}} = 2$, such that 3 input bits are mapped on a subsequence of 2 symbols. Table 2 and Table 3 show the

TABLE 2. *Gray code* for $M_{\text{Rx}} = 3$.

$M_{\text{Rx}} = 3$		
Gray code	$\boldsymbol{c}_{\text{s}}$ $(\rho_{i-1} = 1)$	$\boldsymbol{c}_{\text{s}}$ $(\rho_{i-1} = -1)$
00	1 1 1	−1 −1 −1
01	1 1 −1	−1 −1 1
11	1 −1 −1	−1 1 1
10	−1 −1 −1	1 1 1

TABLE 3. Proposed *Gray code* for $M_{\text{Rx}} = 2$.

$M_{\text{Rx}} = 2$		
Gray Code	$[\boldsymbol{c}_{\text{s},2i}, \boldsymbol{c}_{\text{s},2i+1}]$ $\rho_{2i-1} = 1$	$[\boldsymbol{c}_{\text{s},2i}, \boldsymbol{c}_{\text{s},2i+1}]$ $\rho_{2i-1} = -1$
000	1 1 1 1	−1 −1 −1 −1
001	1 1 1 −1	−1 −1 −1 1
011	1 1 −1 −1	−1 −1 1 1
010	1 −1 −1 −1	−1 1 1 1
110	1 −1 −1 1	−1 1 1 −1
111	−1 −1 −1 1	1 1 1 −1
101	−1 −1 −1 −1	1 1 1 1
100	−1 −1 1 1	1 1 −1 −1

corresponding Gray mapping for $M_{\text{Rx}} = 3$ and $M_{\text{Rx}} = 2$, respectively.

IV. WAVEFORM DESIGN OPTIMIZATION

The proposed waveform design, suitable for systems with 1-bit quantization and oversampling, considers the novel TI ZX modulation [20], in conjunction with the optimization of a set of coefficients. It means that instead of considering binary sequences of samples, the proposed waveform is built by concatenating segment sequences of coefficients that contain zero-crossings at the desired time-instances according to $\boldsymbol{c}_{\text{map}}$.

The proposed waveform design relies on the transmit and receive filters $g_{\text{Tx}}(t)$ and $g_{\text{Rx}}(t)$ which preserve the zero-crossing time-instance. Different to [20], the sequence is no longer binary but is defined by the set of coefficients $\boldsymbol{\mathcal{G}}$ so that each symbol x_i drawn from the set $\mathcal{X}_{\text{in}}$ is mapped into a codeword $\boldsymbol{g}_i$ with M_{Rx} different coefficients which convey the information into the time-instances of zero-crossings. As in the original TI ZX modulation [20], it is considered that sequences are constructed for real and imaginary parts independently. In the following, a real-valued process is described.

The set of optimal coefficients $\boldsymbol{\mathcal{G}}$ with dimensions $n_{\text{s}} \times q$ is defined in terms of $\boldsymbol{\mathcal{G}} = \{\boldsymbol{G}_+; \boldsymbol{G}_-\}$ where $\boldsymbol{G}_- = -\boldsymbol{G}_+$, such that they both convey the same zero-crossings information. In this context, $\boldsymbol{G}_+$ is associated to $\rho = 1$ and $\boldsymbol{G}_-$ is associated to $\rho = -1$.

Considering bit sequences as input and the Gray coding for TI ZX modulation shown in Table 2 and Table 3, q is established such that $q = 3$ for $M_{\text{Rx}} = 3$ and $q = 4$ for $M_{\text{Rx}} = 2$, where q denotes the length of the codeword when Gray coding is considered. In the same way, $n_s = 8$ for $M_{\text{Rx}} = 3$ and $n_s = 16$ for $M_{\text{Rx}} = 2$, where n_s represents the number of different codewords. By considering the symmetry in $\mathcal{G}$, we define the reduced matrices $\boldsymbol{G}_{+/-} = \left[\boldsymbol{g}^T_{1_{+/-}}; \boldsymbol{g}^T_{2_{+/-}}; \cdots; \boldsymbol{g}^T_{ns/2_{+/-}}\right]$, where $\boldsymbol{g}_{i_{+/-}} = \left[g_{i,1_{+/-}}, g_{i,2_{+/-}}, \cdots g_{i,q_{+/-}}\right]$ and $\rho = \text{sgn}\left(g_{i,q}\right)$.

TABLE 4. Set of optimal coefficients $\mathcal{G}$ for $M_{\text{Rx}} = 3$.

$\mathcal{G}$		
$g_{1,1}$	$g_{1,2}$	$g_{1,3}$
$g_{2,1}$	$g_{2,2}$	$-g_{2,3}$
$g_{3,1}$	$-g_{3,2}$	$-g_{3,3}$
$-g_{4,1}$	$-g_{4,2}$	$-g_{4,3}$
$-g_{1,1}$	$-g_{1,2}$	$-g_{1,3}$
$-g_{2,1}$	$-g_{2,2}$	$g_{2,3}$
$-g_{3,1}$	$g_{3,2}$	$g_{3,3}$
$g_{4,1}$	$g_{4,2}$	$g_{4,3}$

In this context the set $\mathcal{G}$ is shown in Table 4 for $M_{\text{Rx}} = 3$ and the matrix $\boldsymbol{G}_+ = -\boldsymbol{G}_-$ for $M_{\text{Rx}} = 3$ is described as

$$\boldsymbol{G}_+ = -\boldsymbol{G}_- = \begin{pmatrix} g_{1,1} & g_{1,2} & g_{1,3} \\ g_{2,1} & g_{2,2} & -g_{2,3} \\ g_{3,1} & -g_{3,2} & -g_{3,3} \\ -g_{4,1} & -g_{4,2} & -g_{4,3} \end{pmatrix} \tag{5}$$

Then, as initially established, the symbol x_i is mapped in the segment $\boldsymbol{g}_{i_{+/-}}$. The pilot sample ρ_{b} is required for the encoding and decoding processes of the first symbol x_1. Finally, the input sequence of symbols $\boldsymbol{x}_k$ is mapped in the sequence $\boldsymbol{s}_{g_k}$ with length N_{tot} by concatenating all the segments $\boldsymbol{g}_{i_{+/-}}$ such that, $\boldsymbol{s}_{g_k} = [\boldsymbol{g}^T_0, \ldots, \boldsymbol{g}^T_{N-1}]^T$. Note that the pilot sample ρ_{b} is predefined and known at the receivers, hence not included in the precoding vector $\boldsymbol{s}_{g_k}$.

A. AUTOCORRELATION FOR TI ZX MODULATION

In this section, it is described how to compute the autocorrelation function of the TI ZX modulated signal, considering the set of coefficients $\boldsymbol{\mathcal{G}}$ which conveys the information into the time-instances of zero-crossings.

To obtain the autocorrelation function, the TI ZX modulation system is converted to a finite-state machine where the current output values are determined only by its current state which corresponds to an equivalent Moore machine [23]. For $M_{\text{Rx}} = 3$, one symbol in terms of two bits is mapped in one output pattern, so $n_{\text{s}} = 8$ different states are presented. While for $M_{\text{Rx}} = 2$ sequences of symbols are considered in terms of mapping three bits segments in four samples, such that there are $n_{\text{s}} = 16$ different states. Table 5 and Table 6 provide the equivalent Moore machine for $M_{\text{Rx}} = 3$ and $M_{\text{Rx}} = 2$, respectively. The states with positive subscripts represent sequences for $\rho = 1$ and states with negative subscripts represent sequences for $\rho = -1$.

Considering a symmetric machine, the matrix $\boldsymbol{\Gamma}$ is defined with m different positive coefficients, where $m = 12$ for $M_{\text{Rx}} = 3$ and $m = 32$ for $M_{\text{Rx}} = 2$.

The state transition probability matrix $\boldsymbol{Q}$ of the equivalent Moore machine, with dimensions $n_{\text{s}} \times n_{\text{s}}$ is defined for i.i.d.

input bits, all valid state transitions have equal probability p with $p = 1/4$ for $M_{\mathrm{Rx}} = 3$ and $p = 1/8$ for $M_{\mathrm{Rx}} = 2$. Furthermore, the vector $\boldsymbol{\pi} = (1/n_{\mathrm{s}})\mathbf{1}$ of length n_{s} corresponds to the stationary distribution of the equivalent Moore machine, which implies $\boldsymbol{\pi}^T\boldsymbol{Q} = \boldsymbol{\pi}^T$. Then, the matrix $\boldsymbol{\Gamma}$ with dimensions $n_{\mathrm{s}} \times M_{\mathrm{Rx}}$ for $M_{\mathrm{Rx}} = 3$ and $n_{\mathrm{s}} \times 2M_{\mathrm{Rx}}$ for $M_{\mathrm{Rx}} = 2$ is defined which contains the Moore machine's output $\boldsymbol{g}_{i_{+/-}}$. The block-wise correlation matrix of the TI ZX mapping output is given by [24, eq. 3.46]

$$\boldsymbol{R}_{\boldsymbol{g}}^{\kappa} = \mathrm{E}\{\boldsymbol{g}_{\kappa'}\boldsymbol{g}_{\kappa'+\kappa}^T\} = \boldsymbol{\Gamma}^T\boldsymbol{\Pi}\boldsymbol{Q}^{|\kappa|}\boldsymbol{\Gamma}. \tag{6}$$

Then, the average autocorrelation function $\boldsymbol{r}_g$ of the TI ZX modulation output sequence can be obtained as [24, eq. 3.39]

$$\boldsymbol{r}_{\boldsymbol{g}}[kq+l] = \frac{1}{q}\left(\sum_{i=1}^{q-l}\left[\boldsymbol{R}_{\boldsymbol{g}}^{k}\right]_{i,l+i} + \sum_{i=q-l+1}^{q}\left[\boldsymbol{R}_{\boldsymbol{g}}^{k+1}\right]_{i,l+i-q}\right), \tag{7}$$

for $k \in \mathbb{Z}$, $0 \le l \le q-1$.

TABLE 5. Equivalent Moore machine for TI ZX mapping for $M_{\mathrm{Rx}} = 3$.

Current state	next state				output
	00	01	11	10	$\boldsymbol{g}_i$
1_+	1_+	2_+	3_+	4_+	$g_{1,1}$ $g_{1,2}$ $g_{1,3}$
2_+	1_-	2_-	3_-	4_-	$g_{2,1}$ $g_{2,2}$ $-g_{2,3}$
3_+	1_-	2_-	3_-	4_-	$g_{3,1}$ $-g_{3,2}$ $-g_{3,3}$
4_+	1_-	2_-	3_-	4_-	$-g_{4,1}$ $-g_{4,2}$ $-g_{4,3}$
1_-	1_-	2_-	3_-	4_-	$-g_{1,1}$ $-g_{1,2}$ $-g_{1,3}$
2_-	1_+	2_+	3_+	4_+	$-g_{2,1}$ $-g_{2,2}$ $g_{2,3}$
3_-	1_+	2_+	3_+	4_+	$-g_{3,1}$ $g_{3,2}$ $g_{3,3}$
4_-	1_+	2_+	3_+	4_+	$g_{4,1}$ $g_{4,2}$ $g_{4,3}$

TABLE 6. Equivalent Moore machine for TI ZX mapping for $M_{\mathrm{Rx}} = 2$.

Current state	next state								output
	000	001	011	010	110	111	101	100	$\boldsymbol{g}_i$
1_+	1_+	2_+	3_+	4_+	5_+	6_+	7_+	8_+	$g_{1,1}$ $g_{1,2}$ $g_{1,3}$ $g_{1,4}$
2_+	1_-	2_-	3_-	4_-	5_-	6_-	7_-	8_-	$g_{2,1}$ $g_{2,2}$ $g_{2,3}$ $-g_{2,4}$
3_+	1_-	2_-	3_-	4_-	5_-	6_-	7_-	8_-	$g_{3,1}$ $g_{3,2}$ $-g_{3,3}$ $-g_{3,4}$
4_+	1_-	2_-	3_-	4_-	5_-	6_-	7_-	8_-	$g_{4,1}$ $-g_{4,2}$ $-g_{4,3}$ $-g_{4,4}$
5_+	1_+	2_+	3_+	4_+	5_+	6_+	7_+	8_+	$g_{5,1}$ $-g_{5,2}$ $-g_{5,3}$ $g_{5,4}$
6_+	1_+	2_+	3_+	4_+	5_+	6_+	7_+	8_+	$-g_{6,1}$ $-g_{6,2}$ $-g_{6,3}$ $g_{6,4}$
7_+	1_-	2_-	3_-	4_-	5_-	6_-	7_-	8_-	$-g_{7,1}$ $-g_{7,2}$ $-g_{7,3}$ $-g_{7,4}$
8_+	1_+	2_+	3_+	4_+	5_+	6_+	7_+	8_+	$-g_{8,1}$ $-g_{8,2}$ $g_{8,3}$ $g_{8,4}$
1_-	1_-	2_-	3_-	4_-	5_-	6_-	7_-	8_-	$-g_{1,1}$ $-g_{1,2}$ $-g_{1,3}$ $-g_{1,4}$
2_-	1_+	2_+	3_+	4_+	5_+	6_+	7_+	8_+	$-g_{2,1}$ $-g_{2,2}$ $-g_{2,3}$ $g_{2,4}$
3_-	1_+	2_+	3_+	4_+	5_+	6_+	7_+	8_+	$-g_{3,1}$ $-g_{3,2}$ $g_{3,3}$ $g_{3,4}$
4_-	1_+	2_+	3_+	4_+	5_+	6_+	7_+	8_+	$-g_{4,1}$ $g_{4,2}$ $g_{4,3}$ $g_{4,4}$
5_-	1_-	2_-	3_-	4_-	5_-	6_-	7_-	8_-	$-g_{5,1}$ $g_{5,2}$ $g_{5,3}$ $-g_{5,4}$
6_-	1_-	2_-	3_-	4_-	5_-	6_-	7_-	8_-	$g_{6,1}$ $g_{6,2}$ $g_{6,3}$ $-g_{6,4}$
7_-	1_+	2_+	3_+	4_+	5_+	6_+	7_+	8_+	$g_{7,1}$ $g_{7,2}$ $g_{7,3}$ $g_{7,4}$
8_-	1_-	2_-	3_-	4_-	5_-	6_-	7_-	8_-	$g_{8,1}$ $g_{8,2}$ $-g_{8,3}$ $-g_{8,4}$

B. WAVEFORM DESIGN

As the signs of the coefficients are predefined by the TI ZX modulation, we optimize the amplitude of the coefficients in the optimization process by introducing the matrix $\boldsymbol{G}$. Let $\boldsymbol{G}$ be a matrix such that $\boldsymbol{G}_{i,j} = |\boldsymbol{G}_{+i,j}| = |\boldsymbol{G}_{-i,j}|$. Then, the matrix $\boldsymbol{G}$, is vectorized such that $\boldsymbol{g}_u = \mathrm{vec}(\boldsymbol{G})$. The vector $\boldsymbol{g}_u$ is later optimized such that with this optimal vector the set $\mathcal{G}$ is shaped to construct the temporal precoding vector $\boldsymbol{s}_g$. The autocorrelation function is calculated with (7) and the PSD is calculated by

$$S(f) = S_x(f)\,|G_{\mathrm{Tx}}(f)|^2, \tag{8}$$

where $G_{\mathrm{Tx}}(f)$ refers to the transfer function of the transmit filter g_{Tx} and $S_x(f)$ to the PSD of the transmit sequence

$$S_x(f) = \frac{M_{\mathrm{Rx}}}{T}\sum_{l=-\infty}^{\infty} c_l e^{j2\pi\frac{lT}{M_{\mathrm{Rx}}}f}, \tag{9}$$

where c_l denotes the l-th element of the autocorrelation function from (7). By defining a critical frequency f_c and a power containment factor η, the inband power is defined as

$$\int_{-f_c}^{f_c} S(f)\mathrm{d}f = \eta P, \tag{10}$$

where $P = \int_{-\infty}^{\infty} S(f)\mathrm{d}f$. Then, when considering $g_{\mathrm{Rx}}(t)$ and $g_{\mathrm{Tx}}(t)$ as rectangular filters,

$$g_{\mathrm{Rx}}(t) = g_{\mathrm{Tx}}(t) = \sqrt{\frac{1}{T/M_{\mathrm{Rx}}}}\,\mathrm{rect}\left(\frac{t}{T/M_{\mathrm{Rx}}}\right), \tag{11}$$

matrix $\boldsymbol{V}$ is as an identity matrix. The absolute value squared of the transfer function is given by

$$|G_{\mathrm{Tx}}(f)|^2 = \frac{T}{M_{\mathrm{Rx}}}\mathrm{sinc}^2\left(f\frac{T}{M_{\mathrm{Rx}}}\right). \tag{12}$$

With this, (8) can be expressed as

$$S(f) = \mathrm{sinc}^2\left(f\frac{T}{M_{\mathrm{Rx}}}\right)\sum_{l=-\infty}^{\infty} c_l e^{j2\pi\frac{lT}{M_{\mathrm{Rx}}}f}. \tag{13}$$

Samples close to the decision threshold are more noise-sensitive. Then, the maximization of the minimum distance to the decision threshold γ is considered as the optimization criterion. With this, an optimization problem that maximizes γ can be formulated as:

$$\begin{aligned} &\text{minimize}_{\boldsymbol{g}_u} \quad -\gamma \\ &\text{subject to} \quad \boldsymbol{g}_u \succeq \gamma\mathbf{1} \\ &\qquad \|\boldsymbol{g}_u\|_2^2 \le m\frac{E_0}{2N_{\mathrm{u}}NM_{\mathrm{Rx}}} \\ &\qquad \eta(\boldsymbol{g}_u, f_c) \ge \delta, \end{aligned} \tag{14}$$

where δ corresponds to the in band power target ratio. Assuming that the optimal solution for $\boldsymbol{g}_u$ fulfills the power constraint with equality, we can make the following statement. Using the optimal set of coefficients $\mathcal{G}$, the sequence $\boldsymbol{s}_{g_k}$ is constructed for each user. Then, the average total power of the complex transmit signal $\boldsymbol{s}_g$ is given by

$$\mathbb{E}\left\{\boldsymbol{s}_g^H\boldsymbol{A}^H\boldsymbol{A}\boldsymbol{s}_g\right\} = E_0, \tag{15}$$

where $\boldsymbol{A} = \boldsymbol{I}_{N_{\mathrm{u}}} \otimes \boldsymbol{G}_{\mathrm{Tx}}^T$ and $\boldsymbol{G}_{\mathrm{Tx}}$ denotes a Toeplitz matrix of size $N_{\mathrm{tot}} \times 3N_{\mathrm{tot}}$, which is given by

$$\boldsymbol{G}_{\mathrm{Tx}} = a_{\mathrm{Tx}}\begin{bmatrix} \left[\boldsymbol{g}_{\mathrm{Tx}}^T\right] & 0\cdots & 0 \\ 0 & \left[\boldsymbol{g}_{\mathrm{Tx}}^T\right] & 0\cdots 0 \\ & \ddots\ddots\ddots & \\ 0\cdots & 0 & \left[\boldsymbol{g}_{\mathrm{Tx}}^T\right] \end{bmatrix}, \tag{16}$$

with $\boldsymbol{g}_{\text{Tx}} = \left[g_{\text{Tx}}(-T(N+M_{\text{Tx}}^{-1})),\ g_{\text{Tx}}(-T(N+M_{\text{Tx}}^{-1})+T\,M_{\text{Tx}}^{-1}),\ldots,g_{\text{Tx}}(T(N+M_{\text{Tx}}^{-1}))\right]^T$ and $a_{\text{Tx}} = (T/M_{\text{Tx}})^{1/2}$. Note that under the assumption in (11), $\boldsymbol{A}^H\boldsymbol{A}$ corresponds to the identity matrix of dimensions $N_{\text{tot}} \times N_{\text{tot}}$. Due to the last constraint in (14) the problem is non convex and it is difficult to find a solution directly.

When no spectral constraint is considered, the maximum value for γ, it is γ_M is reached, and it is obtained by solving the optimization problem

$$\begin{aligned} &\text{minimize}_{\boldsymbol{g}_u} \quad -\gamma \\ &\text{subject to} \quad \boldsymbol{g}_u \succeq \gamma\mathbf{1} \\ &\qquad\qquad \|\boldsymbol{g}_u\|_2^2 \le m\frac{E_0}{2N_{\text{u}}NM_{\text{Rx}}}. \end{aligned} \tag{17}$$

The maximum values γ_M reached by solving (17) corresponds to $\gamma_M = \sqrt{\frac{E_0}{2N_{\text{u}}NM_{\text{Rx}}}}$.

The optimization problem in (14) can be solved more easily with fewer restrictions if it is considered that instead of maximizing γ, the power containment bandwidth factor η is maximized. Then, the next section explains in detail how to find sub-optimal solutions to the optimization problem in (14).

V. A PRACTICAL WAVEFORM DESIGN OPTIMIZATION STRATEGY

This section describes the implementation of the solution to problem (14). Once the oversampling factor M_{Rx} has been defined, an initial vector $\boldsymbol{g}_u = \gamma\mathbf{1}$ of positive coefficients of length $m = 12$ is established. Then the matrix Q of the equivalent Moore machine, which defines the transition probability from one state to another, is established as shown below for $M_{\text{Rx}} = 3$.

$$\boldsymbol{Q} = \frac{1}{4}\begin{bmatrix} 1&1&1&1&0&0&0&0\\ 0&0&0&0&1&1&1&1\\ 0&0&0&0&1&1&1&1\\ 0&0&0&0&1&1&1&1\\ 0&0&0&0&1&1&1&1\\ 1&1&1&1&0&0&0&0\\ 1&1&1&1&0&0&0&0\\ 1&1&1&1&0&0&0&0 \end{bmatrix}. \tag{18}$$

With the initial vector $\boldsymbol{g}_u$ the matrix $\boldsymbol{\Gamma}$ is shaped. Then the matrix $\boldsymbol{\Pi} = \text{diag}(\boldsymbol{\pi})$ is defined. With a maximum value κ established, the average autocorrelation is calculated through equation (7).

To calculate the PSD in (13), a new variable $f_T = fT$ is introduced such that normalized vector $\boldsymbol{f}_T$ is defined as

$$\boldsymbol{f}_T = [0, 0.001, 0.002, \cdots, \lambda].$$

Then the double side average autocorrelation function is shaped by flipping the vector $\boldsymbol{r}_g$ in the left-right direction except for the first sample and concatenating with the original $\boldsymbol{r}_g$ vector. Then, $S(f) = S'(\boldsymbol{f}_T)$ is calculated with (13) using the vector $\boldsymbol{f}_T$.

Algorithm 1 Proposed Algorithm to Solve (14)

1: Define a critical frequency f_c
2: Define $\gamma = \Delta_\gamma$
3: Define an in band power target ratio α
repeat
4: Initialize $\boldsymbol{g}_u = \gamma\mathbf{1}$
repeat
5: solve

$$\begin{aligned} &\text{minimize}_{\boldsymbol{g}_u} \quad -\eta(\boldsymbol{g}_u) \\ &\text{subject to} \quad \|\boldsymbol{g}_u\|_2^2 \le m\frac{E_0}{2N_{\text{u}}NM_{\text{Rx}}} \\ &\qquad\qquad \boldsymbol{g}_u \succeq \gamma\mathbf{1}, \end{aligned}$$

until A feasible solution is found.
6: Increase γ, $\gamma = \gamma + \Delta_\gamma$ in (22)
until $\eta \le \delta$.

The approximate integral P_T of $S(f)$ is computed as:

$$P_T = \int_0^{\lambda/T} S(f)df \approx \frac{\Delta_f}{2}\sum_{n=1}^{N_f}(S'(f_{T,n}) + S'(f_{T,n+1})), \tag{19}$$

where $\Delta_f = \frac{\lambda}{N_f T}$ and $N_f + 1$ corresponds to the length of the vector $\boldsymbol{f}_T$. Then the critical frequency is set to f_c, and the approximate integral P_{f_c} of $S(f) = S'(\boldsymbol{f}_{T_c})$ is calculated for a normalized frequency vector $\boldsymbol{f}_{T_c} = [0, 0.001, \cdots, f_c T]$. Then, the in-band power can be computed as follows

$$P_{f_c} = \int_0^{f_c} S(f)df \approx \frac{\Delta_{f_c}}{2}\sum_{n=1}^{N_c}(S'(f_{T_c,n}) + S'(f_{T_c,n+1})), \tag{20}$$

where $\Delta_{f_c} = \frac{f_c}{N_c T}$ and $N_c + 1$ corresponds to the length of the vector $\boldsymbol{f}_{T_c}$. Next, the power containment factor η is calculated as

$$\eta = \frac{P_{f_c}}{P_T}. \tag{21}$$

With the latter, an equivalent optimization problem to (14) is expressed as:

$$\begin{aligned} &\text{minimize}_{\boldsymbol{g}_u} \quad -\eta(\boldsymbol{g}_u) \\ &\text{subject to} \quad \|\boldsymbol{g}_u\|_2^2 \le m\frac{E_0}{2N_{\text{u}}NM_{\text{Rx}}} \\ &\qquad\qquad \boldsymbol{g}_u \succeq \gamma\mathbf{1}, \end{aligned} \tag{22}$$

where γ corresponds to the minimum value of $\boldsymbol{g}_u$. Practical solutions for the problem in (22) can be found by numerical local optimization. When the optimal value for $\eta > \delta$, then γ can be increased, in terms of $\gamma = \gamma + \Delta_\gamma$ and the process is repeated until the in-band power target ratio δ is reached with approximately equality. The optimization strategy is summarized in Algorithm 1.

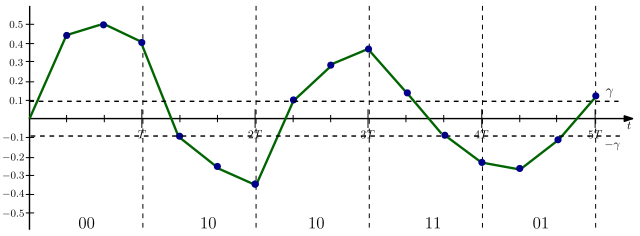

FIGURE 2. Mapping process for construction of s_g with the set of optimal coefficients G for $M_{\text{Rx}} = 3$.

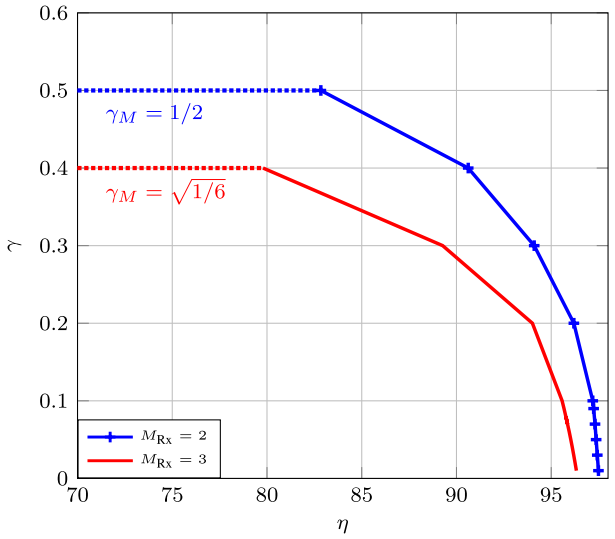

FIGURE 3. γ vs η with $N_{\text{u}} = 1$.

A. DETECTION

The detection process for the proposed waveform, follows the same process as for the existing TI ZX waveforms which aims for a low complexity receiver [20]. The detection process is done in the same way and separately for each user stream. From the sequence received in (1) the corresponding z_k sequences of each user are obtained. The sequence z_k is segmented into subsequences $z_{\text{b}_i} = [\rho_{i-1}, z_i]^T \in \{+1, -1\}^{M_{\text{Rx}}+1}$, where ρ_{i-1} corresponds to the last sample of $z_{\text{b}_{i-1}}$ which corresponds to the received sequence of the $(i-1)$ symbol interval. Then the backward mapping process is define such that $\overleftarrow{d} : z_{\text{b}_i} \rightarrow [\rho_{i-1}, \boldsymbol{c}_{s_i}^T]$ [20]. In the noise free case it is possible to decode the sequence with the backward mapping process $\overleftarrow{d}(\cdot)$. However, in the presence of noise, invalid sequences z_{b_i} may arise that are not possible to detect via $\overleftarrow{d}(\cdot)$. Hence, the Hamming distance metric is required [14] which is defined as

$$\hat{\boldsymbol{x}}_i = \overleftarrow{d}(\boldsymbol{c}), \quad \text{with} \quad \boldsymbol{c} = \arg\min_{\boldsymbol{c}_{\text{map}} \in \mathcal{M}} \text{Hamming}(z_{\text{b}_i}, \boldsymbol{c}_{\text{map}}), \quad (23)$$

where $\text{Hamming}(z_{\text{b}_i}, \boldsymbol{c}_{\text{map}}) = \sum_{n=1}^{M_{\text{Rx}}+1} \frac{1}{2} \left| z_{\text{b}_{i,n}} - \boldsymbol{c}_{\text{map},n} \right|$ and $\boldsymbol{c}_{\text{map}} = [\rho_{i-1}, \boldsymbol{c}_{s_i}]^T$, and $\mathcal{M}$ denotes all valid forward mapping codewords. The detection of the first symbol in the sequence, considers the sample ρ_{b} which then enables the detection process. The real and the imaginary parts are detected independently in separate processes.

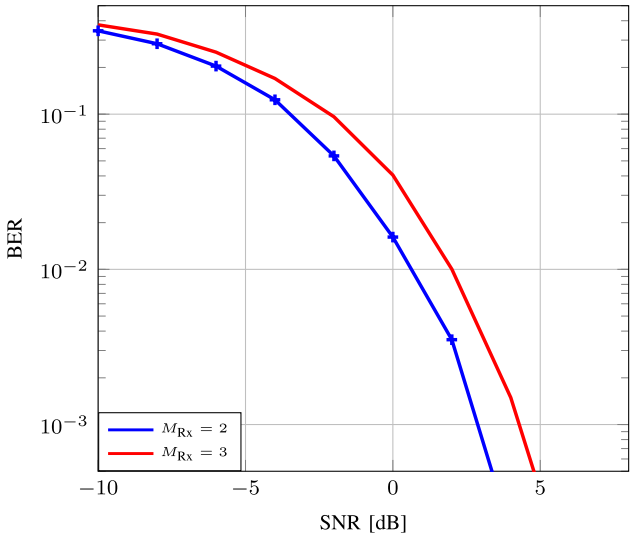

FIGURE 4. BER vs SNR for γ_M with $N_u = 2$.

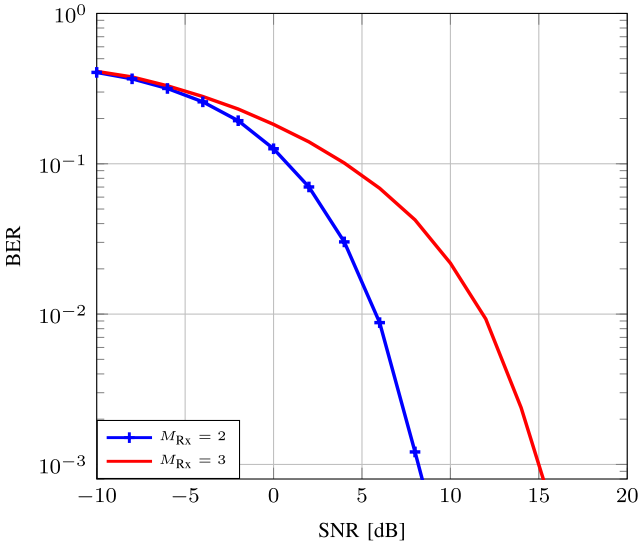

FIGURE 5. BER vs SNR for the proposed waveform with $\delta = 0.95$.

VI. NUMERICAL RESULTS

This section presents numerical results in terms of uncoded BER and normalized PSD for the proposed TI ZX state machine waveform design. Moreover, the proposed technique results are compared with other methods from the literature, namely TI ZX MMDDT [20] and ZX transceiver design [8]. The system under consideration employs $N_{\text{t}} = 8$ transmit antennas and $N_{\text{u}} = 2$ single-antenna users for all the evaluated methods. The SNR is defined as follows:

$$\text{SNR} = \frac{E_0 \text{trace}\left(HH^H\right)}{NTN_0N_{\text{u}}N_{\text{t}}2f_c}, \quad (24)$$

where N_0 denotes the noise power spectral density. The bandwidth B is defined as $B = 2f_c$, where the critical frequency is set to $f_c = 0.65/T$. The entries of the channel matrix $\boldsymbol{H}$ are i.i.d. with $\mathcal{CN}(0, 1)$.

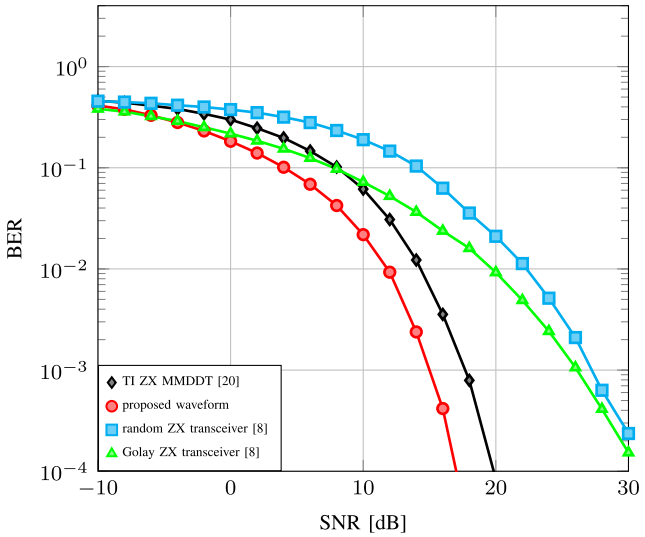

FIGURE 6. BER vs SNR for $M_{\mathrm{Rx}} = 3$ for all the considered methods.

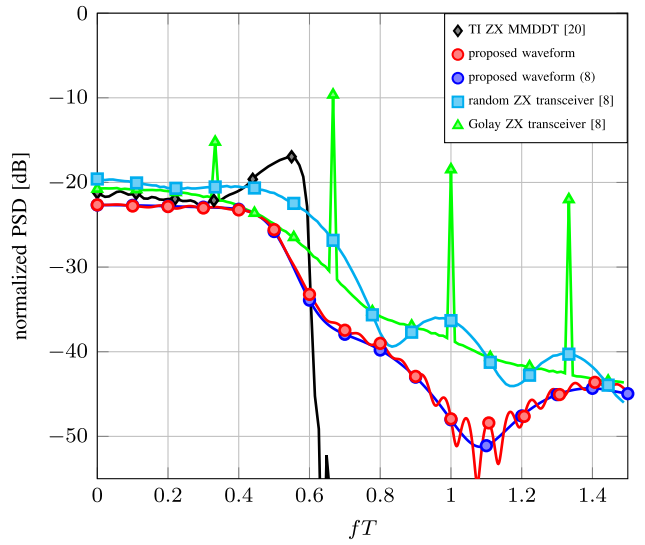

FIGURE 7. PSD for $M_{\mathrm{Rx}} = 3$.

The presented results for the TI ZX MMDDT method from [20] consider $M_{\mathrm{Rx}} = 3$ and the same data rate as for the proposed TI ZX state machine waveform design with $g_{\mathrm{Tx}}(t)$ as an RC filter and $g_{\mathrm{Rx}}(t)$ as an RRC filter with roll-off factors $\epsilon_{\mathrm{Tx}} = \epsilon_{\mathrm{Rx}} = 0.22$, with $f_c = (1+\epsilon_{\mathrm{Tx}})/2T$. On the other hand, for the ZX transceiver design [8], $M_{\mathrm{Rx}} = 3$ is considered for the random and the Golay mapping methods. The truncation interval is set to $\zeta = 3$ and the number of bits per subinterval $n = 2$, and at the receiver an integrate-and-dump-filter is considered [8]. Table 7 presents the simulation parameters considered to solve the optimization problem in (22). On the other hand, Table 8 summarizes the simulation specifications for the proposed TI ZX waveform design and other methods from the literature, where I_{b} corresponds to the number of input bits per user and O_{s} represents the number of samples after the mapping process.

The optimal matrix $\boldsymbol{G}$ of positive coefficients is shown in Table 9 and Table 10 for $M_{\mathrm{Rx}} = 2$ and $M_{\mathrm{Rx}} = 3$, respectively, where the normalization $\frac{E_0}{N} = 1$ is considered for the problems in (14), (17) and (22). The input sequences of symbols $\boldsymbol{x}$ are mapped onto the temporal transmit vector $\boldsymbol{s}_g$ considering the set of coefficients in Table 9 and Table 10 where $N_{\mathrm{u}} = 1$ are considered and $\delta = 0.95$. Moreover, Δ_γ was set to $\Delta_\gamma = 0.1$ for $M_{\mathrm{Rx}} = 3$ and $\Delta_\gamma = 0.001$ for $M_{\mathrm{Rx}} = 2$. Fig. 2 illustrates an example for $M_{\mathrm{Rx}} = 3$, of how the sequence $\boldsymbol{s}_g$ is built taking into account the optimal coefficients $\boldsymbol{G}$ of Table 10. For Fig. 2, it is considered an example of the input sequence of bits $\boldsymbol{x}_k = [0, 0, 1, 0, 1, 0, 1, 1, 0, 1]$ and with the Gray coding shown in Table 2 two bits are mapped in one sequence $\boldsymbol{g}$. The pilot sample is set to $\rho_b = 1$ such that for the first binary tuple 00 the mapped sequence corresponds to $\boldsymbol{g}_{1_+} = [g_{1,1}, g_{1,2}, g_{1,3}] = [0.6592, 0.3531, 0.2237]$. To map the second binary tuple 10, the last sample of $\boldsymbol{g}_{1_+}$ needs to be taken into account, so that $\rho = \mathrm{sgn}(0.2237) = 1$, therefore the mapped sequence corresponds to $\boldsymbol{g}_{4_+} = [-g_{4,1}, -g_{4,2}, -g_{4,3}] = [-0.1823, -0.3117, -0.5094]$. The process is done for the whole sequence $\boldsymbol{x}_k$ and the final sequence $\boldsymbol{s}_g = [\boldsymbol{g}_{1_+}, \boldsymbol{g}_{4_+}, \boldsymbol{g}_{4_-}, \boldsymbol{g}_{3_+}, \boldsymbol{g}_{2_-}]$.

In Fig. 3 the influence of the bandwidth on γ is presented, which confirms that when higher amount of out-of-band radiation is allowed, the optimal γ reaches a higher value. For $M_{\mathrm{Rx}} = 3$ the maximum value for $\gamma_M = 1/\sqrt{6N_{\mathrm{u}}}$ where an 79% of in band radiation is reached. In the case of $M_{\mathrm{Rx}} = 2$ the maximum value for $\gamma_M = 1/(2\sqrt{N_{\mathrm{u}}})$, where an 83% of in band radiation is reached. It is also observed that the case with $M_{\mathrm{Rx}} = 2$ reaches a higher γ value than for $M_{\mathrm{Rx}} = 3$ when achieving the same in-band power. Then, Fig. 4 presents the BER results considering $\gamma_M = 0.35$ for $M_{\mathrm{Rx}} = 2$ and $\gamma_M = 0.28$ $M_{\mathrm{Rx}} = 3$. In the case of $M_{\mathrm{Rx}} = 2$, it shows a better performance since it is based on a higher γ_M value.

Numerical results are also presented in terms of BER for the proposed TI ZX state machine waveform design in Fig. 5 for $M_{\mathrm{Rx}} = 2$ and $M_{\mathrm{Rx}} = 3$. As expected for $M_{\mathrm{Rx}} = 2$ a lower BER is achieved than for $M_{\mathrm{Rx}} = 3$. In both cases, a target power containment factor $\delta = 0.95$ was reached. On the other hand, $\gamma = 0.07$ for $M_{\mathrm{Rx}} = 3$ and $\gamma = 0.17$ for $M_{\mathrm{Rx}} = 2$. In Fig. 6 the BER is evaluated and compared with other methods form the literature for $M_{\mathrm{Rx}} = 3$. The proposed TI ZX state machine waveform design achieves a lower BER than the TI ZX MMDDT [20] while having a lower computational complexity. In this context, the complexity order for the proposed state machine waveform design is dominated by the spatial ZF precoder whose complexity in Big O nation is given by $\mathcal{O}(N_{\mathrm{t}}^3)$. This is because the coefficients are optimized only once for any transmitted sequence of symbols. On the other hand, the complexity order for the TI ZX MMDDT [20] is given by $\mathcal{O}(2N_{\mathrm{u}}(N_{\mathrm{tot}})^{3.5} + N_{\mathrm{t}}^3)$. However, note that the proposed TI ZX state machine waveform design yields a low level of out-of-band-radiation as seen in Fig. 7. Additionally, the proposed method is compared with the transceiver design from [8]. The transceiver design method considers the nonuniform zero-crossing pattern with random and Golay mapping and power containment factor $\eta = 0.95$.

TABLE 7. Parameters values.

Parameter	Value
κ	400
f_c	$0.65/T$
λ	$2M_{\mathrm{Rx}}$
Δ_γ	0.01
δ	0.95

TABLE 8. Simulation parameters.

Method	M_{Rx}	Transmit Filter	Receive filter	I_{b}	O_{s}
TI ZX MMDDT [20]	2	RC $\alpha = 0.22$	RRC $\alpha = 0.22$	45	61
	3			60	91
ZX transceiver design [8]	3	RC window $\alpha = 0.1$	Integrate-and-dump	180	270
TI ZX waveform design	2	Integrator T/M_{Rx}	Integrator T/M_{Rx}	45	60
	3			60	90

TABLE 9. Optimal set G for $M_{\mathrm{Rx}} = 2$ with $N_{\mathrm{u}} = 1$ and $\delta = 0.95$.

	G				
g_1	000	0.8176,	0.5430,	0.4428,	0.25
g_2	001	0.25,	0.25,	0.25,	0.25
g_3	011	0.19,	0.5461,	0.25,	0.25
g_4	010	0.25,	0.5131,	0.6711,	0.25
g_5	110	1.1826,	0.25,	0.25,	0.25
g_6	111	0.25,	0.25,	0.7025,	0.25
g_7	101	0.7287,	0.25,	0.3715,	0.4114
g_8	100	0.25,	0.25,	0.462,	0.424

TABLE 10. Optimal set G for $M_{\mathrm{Rx}} = 3$ with $N_{\mathrm{u}} = 1$ and $\delta = 0.95$.

	G			
g_1	00	0.6592,	0.3531,	0.2237
g_2	01	0.1,	0.6986,	0.1
g_3	11	0.1,	0.3724,	0.5866
g_4	10	0.1823	0.3117	0.5094

The proposed TI ZX state machine BER performance is better than the transceiver design [8] when both allow the same level of out-of-band radiation since the concatenation of the codewords which conveys the zero-crossing information for TI ZX method is done considering the sign of the last coefficient of the previous Nyquist Interval. The latter implies a lower number of zero-crossings on average, which can be understood as a relaxation in the waveform design. The concatenation process for the TI ZX method is different from the method in [8] which does not consider the state of the previous Nyquist Interval.

Simulation results are presented also in terms of the normalized PSD. In Fig. 7 the analytical and numerical PSD are compared for the proposed TI ZX state machine waveform design with $M_{\mathrm{Rx}} = 3$. The analytical PSD is calculated with (8) considering the autocorrelation function in (7). In Fig. 7, the normalized PSD of the proposed waveform design is also compared with the normalized PSD of the methods from the literature which is calculated by

$$\mathrm{PSD}_{\mathrm{dB}} = 10\log_{10}\left[O_{\mathrm{s}}^{(-1)}\mathrm{E}\{|F_i|^2\}\right], \tag{25}$$

where F_i is the discrete Fourier transform of the normalized temporal transmit signal per user.

VII. CONCLUSION

In this study, we have developed a TI ZX state machine waveform based on the novel TI ZX modulation for multi-user MIMO downlink systems, with 1-bit quantization and oversampling. The waveform design considers the optimization of a set of coefficients that conveys the information into the time-instances of zero-crossings. The optimization is performed considering the power containment bandwidth and the maximization of the minimum distance to the decision threshold. The simulation results were compared with methods from the literature which employ techniques based on zero-crossings. The BER performance is favorable for the proposed method which achieves a comparable BER result as the TI ZX MMDDT [20] method but with significantly lower computational complexity.

REFERENCES

[1] R. H. Walden, "Analog-to-digital converter survey and analysis," *IEEE J. Sel. Areas Commun.*, vol. 17, no. 4, pp. 539–550, Apr. 1999.
[2] S. Shamai (Shitz), "Information rates by oversampling the sign of a bandlimited process," *IEEE Trans. Inf. Theory*, vol. 40, no. 4, pp. 1230–1236, Jul. 1994.
[3] L. Landau, M. Dörpinghaus, and G. P. Fettweis, "1-bit quantization and oversampling at the receiver: Communication over bandlimited channels with noise," *IEEE Commun. Lett.*, vol. 21, no. 5, pp. 1007–1010, May 2017.
[4] L. T. N. Landau, M. Dörpinghaus, and G. P. Fettweis, "1-bit quantization and oversampling at the receiver: Sequence-based communication," *EURASIP J. Wireless Commun. Netw.*, vol. 2018, no. 1, Apr. 2018.
[5] H. Son, H. Han, N. Kim, and H. Park, "An efficient detection algorithm for PAM with 1-Bit quantization and time-oversampling at the receiver," in *Proc. IEEE 90th Veh. Technol. Conf. (VTC-Fall)*, Honolulu, HI, USA, Sep. 2019, pp. 1–5.
[6] C. Forsch, P. Zillmann, O. Alrabadi, S. Brueck, and W. Gerstacker, "Performance analysis of 1-bit quantization with oversampling for higher-order constellations," in *Proc. IEEE Latin-Amer. Conf. Commun. (LATINCOM)*, Nov. 2022, pp. 1–6.
[7] L. Landau, S. Krone, and G. Fettweis, "Intersymbol-interference design for maximum information rates with 1-Bit quantization and oversampling at the receiver," in *Proc. 9th Int. ITG Conf. Syst., Commun. Coding*, Munich, Germany, Jan. 2013, pp. 1–6.
[8] R. Deng, J. Zhou, and W. Zhang, "Bandlimited communication with one-bit quantization and oversampling: Transceiver design and performance evaluation," *IEEE Trans. Commun.*, vol. 69, no. 2, pp. 845–862, Feb. 2021.
[9] P. Neuhaus, M. Dörpinghaus, H. Halbauer, S. Wesemann, M. Schlüter, F. Gast, and G. Fettweis, "Sub-THz wideband system employing 1-bit quantization and temporal oversampling," in *Proc. IEEE Int. Conf. Commun. (ICC)*, Jun. 2020, pp. 1–7.
[10] P. Neuhaus, M. Dörpinghaus, H. Halbauer, V. Braun, and G. Fettweis, "On the spectral efficiency of oversampled 1-bit quantized systems for wideband LOS channels," in *Proc. IEEE 31st Annu. Int. Symp. Pers., Indoor Mobile Radio Commun.*, Aug. 2020, pp. 1–6.
[11] H. Naaman, S. Mulleti, and Y. C. Eldar, "FRI-TEM: Time encoding sampling of finite-rate-of-innovation signals," *IEEE Trans. Signal Process.*, vol. 70, pp. 2267–2279, 2022.
[12] A. B. Üçüncü, E. Björnson, H. Johansson, A. Ö. Yılmaz, and E. G. Larsson, "Performance analysis of quantized uplink massive MIMO-OFDM with oversampling under adjacent channel interference," *IEEE Trans. Commun.*, vol. 68, no. 2, pp. 871–886, Feb. 2020.
[13] Z. Shao, L. T. N. Landau, and R. C. de Lamare, "Dynamic oversampling for 1-bit ADCs in large-scale multiple-antenna systems," *IEEE Trans. Commun.*, vol. 69, no. 5, pp. 3423–3435, May 2021.
[14] A. Gokceoglu, E. Björnson, E. G. Larsson, and M. Valkama, "Spatio-temporal waveform design for multiuser massive MIMO downlink with 1-bit receivers," *IEEE J. Sel. Topics Signal Process.*, vol. 11, no. 2, pp. 347–362, Mar. 2017.

[15] P. Neuhaus, D. M. V. Melo, L. T. N. Landau, R. C. de Lamare, and G. Fettweis, "Zero-crossing modulations for a multi-user MIMO downlink with 1-bit temporal oversampling ADCs," in *Proc. 29th Eur. Signal Process. Conf. (EUSIPCO)*, Dublin, Ireland, Aug. 2021, pp. 816–820.
[16] L. T. N. Landau and R. C. de Lamare, "Branch-and-bound precoding for multiuser MIMO systems with 1-bit quantization," *IEEE Wireless Commun. Lett.*, vol. 6, no. 6, pp. 770–773, Dec. 2017.
[17] H. Jedda, A. Mezghani, A. L. Swindlehurst, and J. A. Nossek, "Quantized constant envelope precoding with PSK and QAM signaling," *IEEE Trans. Wireless Commun.*, vol. 17, no. 12, pp. 8022–8034, Dec. 2018.
[18] J. Mo and R. W. Heath Jr., "Capacity analysis of one-bit quantized MIMO systems with transmitter channel state information," *IEEE Trans. Signal Process.*, vol. 63, no. 20, pp. 5498–5512, Oct. 2015.
[19] R. Liu, M. Li, Q. Liu, and A. L. Swindlehurst, "Joint symbol-level precoding and reflecting designs for IRS-enhanced MU-MISO systems," *IEEE Trans. Wireless Commun.*, vol. 20, no. 2, pp. 798–811, Feb. 2021.
[20] D. M. V. Melo, L. T. N. Landau, R. C. De Lamare, P. F. Neuhaus, and G. P. Fettweis, "Zero-crossing precoding techniques for channels with 1-bit temporal oversampling ADCs," *IEEE Trans. Wireless Commun.*, vol. 22, no. 8, pp. 5321–5336, Aug. 2023.
[21] D. M. V. Melo, L. T. N. Landau, L. N. Ribeiro, and M. Haardt, "Iterative MMSE space-time zero-crossing precoding for channels with 1-bit quantization and oversampling," in *Proc. 54th Asilomar Conf. Signals, Syst., Comput.*, Pacific Grove, CA, USA, Nov. 2020, pp. 496–500.
[22] D. M. V. Melo, L. T. N. Landau, L. N. Ribeiro, and M. Haardt, "Time-instance zero-crossing precoding with quality-of-service constraints," in *Proc. IEEE Stat. Signal Process. Workshop (SSP)*, Rio de Janeiro, Brazil, Jul. 2021, pp. 121–125.
[23] P. Neuhaus, M. Dörpinghaus, and G. Fettweis, "Zero-crossing modulation for wideband systems employing 1-bit quantization and temporal oversampling: Transceiver design and performance evaluation," *IEEE Open J. Commun. Soc.*, vol. 2, pp. 1915–1934, 2021.
[24] K. A. S. Immink, *Codes for Mass Data Storage*. Eindhoven, The Netherlands: Shannon Found, 2004.

DIANA MARCELA V. MELO (Member, IEEE) was born in Valle del Guamuez, Colombia, in 1994. She received the Diploma degree in electronic engineering from the University of Nariño, Colombia, in 2018, and the M.Sc. degree in communications systems from the Department of Electrical Engineering, Pontifical Catholic University of Rio de Janeiro (PUC-Rio), Brazil, in 2020, where she is currently pursuing the Ph.D. degree in electrical engineering. Her research interests include communications and signal processing.

LUKAS T. N. LANDAU (Senior Member, IEEE) received the B.Sc. and M.Sc. degrees in electrical engineering and information technology from the Ilmenau University of Technology, Germany, in 2009 and 2011, respectively, and the Ph.D. degree in electrical engineering and information technology from Technische Universität Dresden, Germany, in 2016. Since 2016, he has been with the Center for Studies in Telecommunications, Pontifical Catholic University of Rio de Janeiro, Brazil, where he is currently an Adjunct Professor. His research interests include communications and signal processing. He serves as an Associate Editor for IEEE Wireless Communications Letters and the *EURASIP Journal on Wireless Communications and Networking*.

RODRIGO C. DE LAMARE (Senior Member, IEEE) was born in Rio de Janeiro, Brazil, in 1975. He received the Diploma degree in electronic engineering from the Federal University of Rio de Janeiro, in 1998, and the M.Sc. and Ph.D. degrees in electrical engineering from the Pontifical Catholic University of Rio de Janeiro (PUC-Rio), in 2001 and 2004, respectively. Since January 2006, he has been with the Communications Group, School of Physics, Engineering and Technology, University of York, U.K., where he is currently a Professor. Since April 2013, he has also been a Professor with PUC-Rio. His research interests include communications and signal processing, in which he has published more than 500 papers in international journals and conferences. He is an elected member of the IEEE Signal Processing for Communications and Networking Committee. He served as an Editor for IEEE Wireless Communications Letters and IEEE Transactions on Communications.